The Astrophysical Journal, 687:1004–1018, 2008 November 10

THE LARGE BINOCULAR TELESCOPE PANORAMIC VIEW OF THE RECENT STAR FORMATION ACTIVITY IN IC 2574

A. Pasquali, A. Leroy, H.-W. Rix, F. Walter, and T. Herbst
Max-Planck-Institut für Astronomie, Königstuhl 17, D-69117 Heidelberg, Germany

E. Giallongo
INAF—Osservatorio Astronomico di Roma, Via Frascati 33, I-00040 Monteporzio, Roma, Italy

R. Ragazzoni and A. Baruffolo
INAF—Osservatorio Astronomico di Padova, Vicolo dell'Osservatorio 5, I-35122 Padova, Italy

R. Speziali
INAF—Osservatorio Astronomico di Roma, Via Frascati 33, I-00040 Monteporzio, Roma, Italy

J. Hill
Large Binocular Telesope Observatory, University of Arizona, 933 North Cherry Avenue, Tucson, AZ 85721-0065

G. Beccari
Dipartimento di Astronomia, Universitá di Bologna, Via Ranzani 1, I-40127 Bologna, Italy

N. Bouché and P. Buschkamp
Max-Planck-Institut für Extraterrestrische Physik, Giessenbachstrasse, D-85748 Garching, Germany

C. Kochanek
Department of Astronomy, The Ohio State University, 140 West 18th Avenue, Columbus, OH 43210;
and Center for Cosmology and AstroParticle Physics, The Ohio State University,
191 West Woodruff Avenue, Columbus, OH 43210

E. Skillman
Department of Astronomy, University of Minnesota, 116 Church Street SE, Minneapolis, MN 55455

and

J. Bechtold
Steward Observatory, University of Arizona, 933 North Cherry Avenue, Tucson, AZ 85721-0065
Received 2008 March 28; accepted 2008 July 1

ABSTRACT

We present deep imaging of the star-forming dwarf galaxy IC 2574 in the M81 group taken with the Large Binocular Telescope (LBT) in order to study in detail the recent star formation history of this galaxy and to constrain the stellar feedback on its H I gas. We identify the star-forming areas in the galaxy by removing a smooth disk component from the optical images. We construct pixel-by-pixel maps of stellar age and stellar mass surface density in these regions by comparing their observed colors with simple stellar populations synthesized with Starburst99. We find that an older burst occurred about 100 Myr ago within the inner 4 kpc and that a younger burst happened in the last 10 Myr mostly at galactocentric radii between 4 and 8 kpc. We analyze the stellar populations residing in the known H I holes of IC 2574. Our results indicate that, even at the remarkable photometric depth of the LBT data, there is no clear one-to-one association between the observed H I holes and the most recent bursts of star formation in IC 2574. The stellar populations formed during the younger burst are usually located at the periphery of the H I holes and are seen to be younger than the holes' dynamical age. The kinetic energy of hole expansion is found to be, on average, 10% of the total stellar energy released by the stellar winds and supernova explosions of the young stellar populations within the holes. With the help of control apertures distributed across the galaxy we estimate that the kinetic energy stored in the H I gas in the form of its local velocity dispersion is about 35% of the total stellar energy.

Subject headings: galaxies: dwarf — galaxies: fundamental parameters — galaxies: individual (IC 2574) — galaxies: photometry — galaxies: stellar content

1. INTRODUCTION

It is common to summarize how stars form from the neutral gas reservoir of a galaxy and how they evolve and affect the ambient interstellar medium (ISM) with the term "star formation." Through their winds and supernova explosions, stars release kinetic energy and freshly synthesized metals to the ISM, with the possible effect of locally suppressing the formation of new stars and triggering it on somewhat larger scales across their host galaxy (i.e., stellar feedback). The global properties of disk galaxies have been extensively studied by now, and it has been found that the average star formation rate (SFR) of a galaxy tightly correlates with its gas surface density (Schmidt 1959, 1963; Kennicutt 1998a, 1998b). This important result alone, however, does not put strong constraints on the physics of star formation itself; it has indeed been shown that different mechanisms can produce this observed correlation (e.g., Silk 1997; Kennicutt 1998b; Elmegreen 2002). Moreover, our knowledge of star formation is mainly based on local disk galaxies, chemically and dynamically different from local dwarf irregulars, which sometimes undergo

intense starbursts (Heckman 1998). Because of their size and low metallicity, dwarf galaxies are considered to be the local analogs to the galaxy population at high redshift, where starbursts are observed to be a rather recurrent phenomenon (Steidel et al. 1996; Pettini et al. 2001; Blain et al. 2002; Scott et al. 2002). Therefore, understanding the details of star formation in nearby galaxies of different Hubble types is crucial for bootstrapping theories of galaxy formation and evolution. This is now made possible by a new generation of instruments which provide high angular resolution throughout the whole spectral range, especially for observations of atomic H gas at 21 cm (H I). These new data allow us to spatially resolve the star formation activity and gas distribution within a galaxy and to analyze their correlation on small scales and across a wide range of local physical conditions. This approach has recently been applied by Kennicutt et al. (2007) to M51a and to a larger sample of galaxies by Bigiel et al. (2008) and Leroy et al. (2008).

In this paper, we apply a similar method to the dwarf galaxy IC 2574 with the aim of describing its star formation activity (i.e., the age and mass surface density of its stellar populations) and comparing those properties with the ISM (i.e., H I) on an $\simeq$100 pc scale.

IC 2574 (UGC 5666, DDO 81) is a gas-rich dwarf actively forming stars in the M81 group. Miller & Hodge (1994) observed it in Hα emission and identified 289 H II regions, each about 50 pc in diameter. The largest complex of star-forming regions is located in the northeast part of the galaxy (also known as an "H I supergiant shell"; Walter et al. 1998; Walter & Brinks 1999). The authors estimated a global SFR of $\simeq 0.08\,M_{\odot}\,\mathrm{yr}^{-1}$ and concluded that IC 2574 is forming stars at roughly its average rate. Follow-up spectroscopy on some H II regions in the northeast complex by Tomita et al. (1998) showed that the Hα velocity field is chaotic in all regions except two (IC 2574-I and IC 2574-IV), which are characterized by a V-shaped velocity distribution. This V-shaped feature is usually representative of stellar winds blowing out the ISM. Interestingly enough, Drissen et al. (1993) found three candidate Wolf-Rayet (WR) stars in IC 2574-I. WR stars are evolved massive stars known to develop stellar winds stronger than O stars of the same luminosity and to make up as much as 50% of the total mass and kinetic energy released by all massive stars into the ISM (see Leitherer et al. 1992). Therefore, their presence in IC 2574-I can well explain the bulk motion observed in this H II region, as well as date the region to be a few Myr old, given that the WR phase is as short as 2–5 Myr (Robert et al. 1993).

The most intriguing property of IC 2574 is, however, the spatial distribution of its neutral ISM. The high-resolution VLA observations of IC 2574 have resulted in a very structured H I map, with 48 holes ranging in size from $\sim$100 to $\sim$1000 pc. These features appear to be expanding with a radial velocity of about 10 km s^{-1}, which, in turn, defines dynamical ages and kinetic energies consistent with being driven by stellar winds and supernova explosions (Walter & Brinks 1999). In particular, the comparison of the H I map with ultraviolet (UIT) and optical images has revealed that the H II regions located in the northeast complex are distributed along the rim of the H I supergiant shell, and the shell itself is devoid of neutral and ionized gas and possibly filled with hot X-ray gas (Walter et al. 1998). Stewart & Walter (2000) identified a star cluster within the supergiant shell with no associated Hα emission and an age (11 Myr) comparable to the shell dynamical age of 14 Myr. They dated the Hα-emitting rim of the shell to be about 3 Myr old. The authors thus concluded that the H I supergiant shell was created by this star cluster, and shell expansion triggered star formation activity along its rim. As pointed out by Walter & Brinks (1999), the occurrence of Hα emission along the rim of a H I feature is common to all the H I holes found in IC 2574, even if no remnant central star cluster has been identified so far. The question is then whether these holes are the result of stellar feedback, as in the case of the supergiant shell, or are produced by different mechanisms. The data collected so far for the Magellanic Clouds (Kim et al. 1999; Hatzidimitriou et al. 2005), M31 and M33 (see van der Hulst 1996), and Holmberg II (Rhode et al. 1999) offer very little support for a one-to-one correlation between H I holes and OB associations, although the kinetic energy of the hole expansion is consistent with the expansion being triggered by the total energy released by a single stellar population (SSP). One possible explanation that has been put forward is that at least some H I holes (especially those with no indication of recent star formation) may have been produced by mechanisms unrelated to young stars. For example, Loeb & Perna (1998) and Efremov et al. (1998) suggest they arise from gamma-ray bursts. H I holes may also be produced by the collision of high-velocity clouds of neutral gas with the galactic disk (see Tenorio-Tagle 1980, 1981) or, more simply, by the intrinsic turbulence of the ISM (Elmegreen & Efremov 1998; Dib et al. 2006). Rhode et al. (1999) proposed the intergalactic UV radiation field as an additional mechanism to create holes in the H I gas by keeping it ionized (at least in the outskirts of the galactic disk, where the H I volume density is lower), while Bureau & Carignan (2002) suggested that the H I holes detected in Holmberg II may have formed by ram pressure from the intragroup medium.

One could also imagine that the lack of a one-to-one correlation between H I holes and OB associations may be due to the limited photometric depth of the data. For example, Rhode et al. (1999) reached a limiting magnitude $B \simeq 23$ mag in Holmberg II and may have failed to detect fainter young stars (i.e., late-B spectral types). We have taken advantage of the high sensitivity and wide field of view of the LBC-Blue mounted on the Large Binocular Telescope (LBT) to perform deep optical imaging, study in detail the stellar populations in IC 2574, and investigate the possible stellar origin of the H I holes in this galaxy. Our aim is to identify low-luminosity star clusters within these features and establish how their stellar content may be different from any other position across the galaxy and whether the energy budget of the young stars in the H I holes can account for the kinetic energy of these structures. This study allows us to also derive the star formation history of IC 2574 locally, at different galactocentric radii, and in correspondence with different H I column densities. The observations and data reduction are described in § 2. The high-resolution optical morphology of IC 2574 is presented in § 3, while the stellar ages and masses resulting from our dating technique are discussed in § 4. We describe the stellar populations associated with the H I holes in § 5 and draw our conclusions in § 6.

2. OBSERVATIONS

The observations presented here were carried out with the LBT, located on Mount Graham, Arizona (Hill et al. 2006). IC 2574 was observed as part of the Science Demonstration Time for the LBT blue camera (LBC-Blue; Ragazzoni et al. 2006; Giallongo et al. 2008), a wide-field imager with a $23' \times 23'$ field of view and an angular scale of $0.23''$ pixel^{-1}. LBC-Blue is optimized for high throughput across the spectral range from 3200 to 5000 Å and has four CCD detectors of 2048×4608 pixels each. Its filter set includes the Bessel U, B, and V filters plus the g and r bands. At the distance of IC 2574, 4.02 Mpc (Walter et al. 2007), one LBC-Blue pixel corresponds to about 4.4 pc.

IC 2574 was imaged with the LBC-Blue on 2007 February 17, 19, 21, and 22 using a circular dithering pattern ($40''$ in radius)

FIG. 1.—Color composite of IC 2574 obtained with the LBC-Blue in the Bessel *U* (*blue*), *B* (*green*), and *V* (*red*) filters during the Science Demonstration Time of 2007 February. North is up and east to the left. The size of the image is $14' \times 11'$ and corresponds to the central one-fourth of the LBC field of view.

with four different pointings in order to also cover the three intra-CCD gaps (about 16″ each) in the LBC-Blue field of view. The total exposure time was 70 minutes (14×300 s) in the *U* band, 35 minutes (7×300 s) in the *B* band, and 15 minutes (3×300 s) in the *V* band, with an average seeing of $\sim$1.0″. The individual images were reduced with standard IRAF[1] routines. They were corrected for bias and flat-fielding and then aligned to the same pixel grid using GEOMAP and GEOTRAN with an accuracy of better than 0.2 pixels. After background subtraction, the images obtained for the same filter were weighted by their seeing (weight = $\sigma^2_{\rm image}/\sigma^2_{\rm best}$, where $\sigma^2_{\rm best}$ is the best seeing measured for each filter data set) and averaged. The astrometric solution of these combined images was updated using the package Astrometry.net[2] (D. Lang et al. 2008, in preparation). We applied the flux calibration derived by the LBC-Blue team during commissioning to the combined images and checked the consistency of these color transformations on standard stars imaged at the same epoch as IC 2574. The systematic error of the flux calibration turned out to be $\sim$0.03 mag in each band. The combined images reached a limiting surface brightness of 26 mag arcsec^{-2} (in the Vegamag system) at a signal-to-noise ratio (S/N) of 5 in each filter.

In what follows, the LBT optical data collected for IC 2574 are used together with the observations in atomic H gas (H I at 21 cm) performed by Walter & Brinks (1999) with the VLA in its B, C, and D configurations. The H I observations were carried out with a 1.56 MHz bandwidth centered at a heliocentric velocity of 38 km s^{-1}, for a velocity resolution of 2.6 km s^{-1} and an angular resolution of about 7″. The H I map defines a maximum rotation velocity of 70 km s^{-1} at a galactocentric distance of 8 kpc (Oh et al. 2008) and an average velocity dispersion of 7 km s^{-1} (Walter & Brinks 1999).

3. THE OPTICAL MORPHOLOGY OF IC 2574

The color composite of IC 2574 obtained with the LBC-Blue during the Science Demonstration Time of 2007 February is shown in Figure 1, with the *U*, *B*, and *V* images color-coded in blue, green, and red, respectively. The size of the color composite in Figure 1 is $14' \times 11'$ and covers only a quarter of the full

[1] IRAF is distributed by the National Optical Astronomy Observatory, which is operated by the Association of Universities for Research in Astronomy, Inc., under cooperative agreement with the National Science Foundation.

[2] Available at http://astrometry.net.

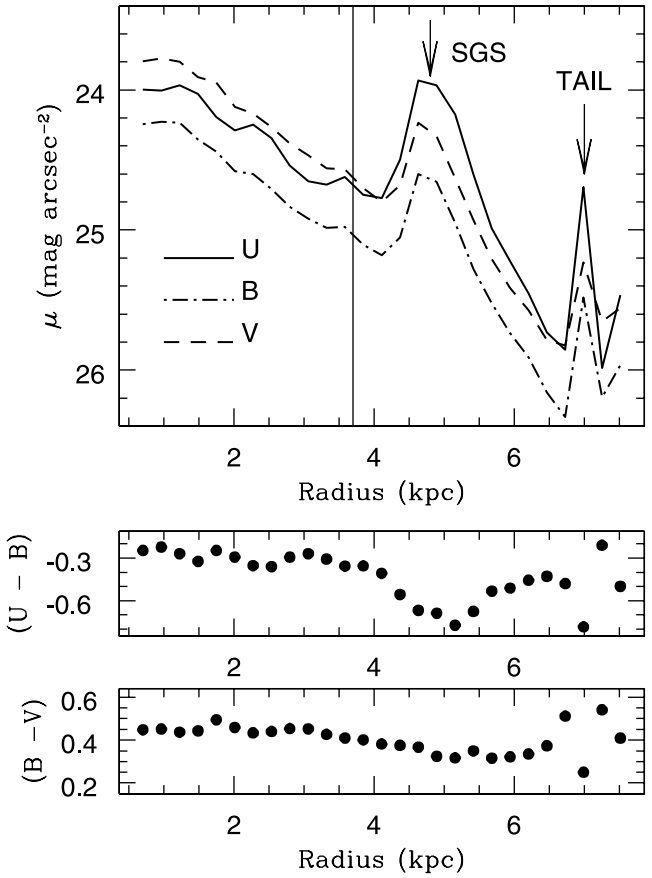

FIG. 2.—Surface brightness profile computed in the U, B, and V bands, together with the radial profile of the $(U - B)$ and $(B - V)$ colors. The surface brightness is corrected for inclination and Galactic extinction. The colors are also corrected for Galactic extinction. The vertical line indicates the scale length of IC 2574, $R_0 = 3.7$ kpc.

field of view of the camera. The combination of high sensitivity with the wide field of view of the camera reveals a wealth of features: the "finger," a knotty tidal stream (oriented east-west); the northeast complex of H II regions (the H I supergiant shell); and the extended tail of star formation in the southwest. Faint plumes of stars departing from the eastern and western sides of IC 2574 are also visible. The star formation activity in IC 2574 appears to mostly occur in the outskirts of the galaxy in a ringlike substructure. This is reminiscent of the optical morphology of the Large Magellanic Cloud (LMC), which, like IC 2574, is a barred late-type galaxy.

From the isophote corresponding to a limiting surface brightness of 26 mag arcsec^{-2} we measure an overall extension for IC 2574 of about 16×7 kpc, which includes the east-west tidal stream and the southwest tail. The ellipse that best fits the $\mu = 26$ isophote is characterized by an axis ratio $q = b/a = 0.47$ and a position angle P.A. $= 55^\circ$. For a disk of intrinsic flattening of $q_0 = 0.12$ (see Martimbeau et al. 1994), this implies an inclination $i = 63^\circ$. With these orientation parameters, we compute the surface brightness profile for concentric elliptical annuli of fixed q and P.A. in each band. These profiles are plotted in Figure 2, where the surface brightness is corrected for inclination (assuming no dust) and Galactic extinction [$E(B - V) = 0.036$ mag; Schlegel et al. 1998] using the extinction law of Cardelli et al. (1989). These profiles nicely follow an exponential disk out to $R \simeq 4$ kpc, with an excess of emission at $R \simeq 5$ and 7 kpc (see Fig. 1). The parameters of the best-fitting exponential disk are listed in Table 1 for each filter, where the central surface brightness (μ_0) is corrected for inclination and the total observed magnitude (m_T) is corrected for Galactic extinction (m_T^0). The mean scale length computed from the LBT data is $R_0 \simeq 3.7$ kpc and agrees well with the scale length (3.2 kpc) obtained by Martimbeau et al. (1994; adopting the same distance). The inner disk (at $R < 4$ kpc) is characterized by a mean $(B - V) \simeq 0.44$ mag and a mean $(U - B) \simeq -0.3$ mag (both corrected for Galactic extinction). In a model of an instantaneous starburst (i.e., a SSP) computed with Starburst99 (Leitherer et al. 1999) for a metallicity similar to that of the Small Magellanic Cloud (SMC), these colors translate to an age of $\sim$1 Gyr and 120 Myr, respectively.

TABLE 1
EXPONENTIAL DISK PARAMETERS

Parameter	U	B	V
μ_0 (mag arcsec^{-2})	23.72	23.94	23.47
R_0 (kpc)	4.1	3.6	3.4
m_T (mag)	10.67	11.13	10.70
m_T^0 (mag)	10.49	10.98	10.59

Figure 3 compares the $\mu = 26$ U-band isophotal contour (*white line*) to the H I distribution to illustrate the spatial relationship between the young stars and the reservoir of atomic gas. The gray scale becomes darker as the column density of the H I gas increases from 5×10^{20} to about 5×10^{21} cm^{-2} (not corrected for inclination). While the H I and U-band light distributions share nearly the same major axis, their minor axes are quite different, with the minor axes being smaller in the optical. This could be due to differences in the scale height of the U-band light and H I distributions.

4. STELLAR POPULATIONS

In order to derive the star formation history of IC 2574 over the last few 10^8 yr from the observed photometry, we need to

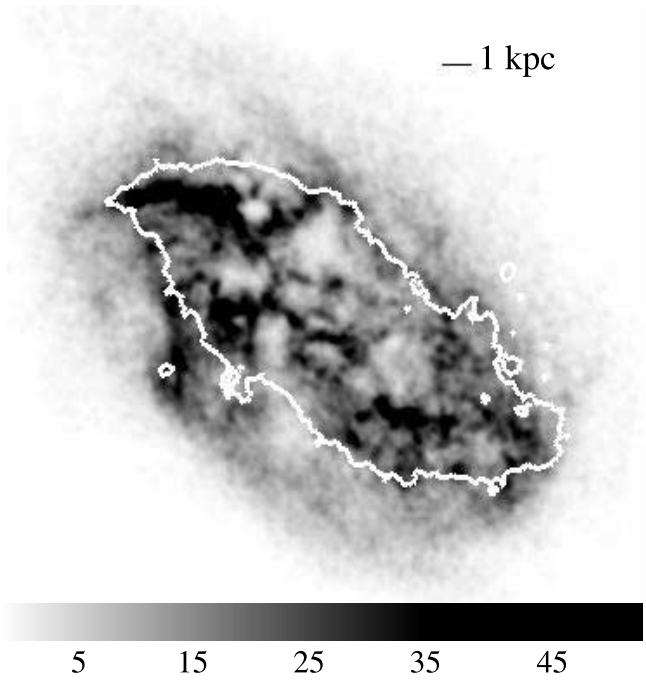

FIG. 3.—Isophotal contour of IC 2574 in the U band corresponding to $\mu_U = 26$ mag arcsec^{-2} (*white line*), superposed on the map of the H I column density in gray (from Walter & Brinks 1999). The gray scale becomes darker as the column density increases from 5×10^{20} to about 5×10^{21} cm^{-2}.

disentangle the colors of star-forming regions from those of the underlying smooth disk, which includes light from older episodes of star formation (see § 3). This is analogous to subtracting the local background in stellar photometry. We first identify the star-forming regions as those bluer than $(U - B) = -0.3$ mag and with a S/N per pixel larger than 5 (in all filters). These regions are likely to contain mostly light from young stars (younger than $\simeq$100 Myr for a SSP synthesized with Starburst99 assuming an SMC-like metallicity). We mask these regions and then fit the remaining light. We fix the galaxy center, ellipticity $(1 - q = 0.53)$, and position angle (55°) and fit the U-band image together with the mask frame using the IRAF routine ELLIPSE. This yields an estimate of the diffuse light across the galaxy, and we subtract this model disk component from the original U image. The residual image should contain only young stars, and we use it in the subsequent analysis. Figure 4 shows, as an example of the whole procedure, the original U image (*top*), the model disk component with the masked regions overlaid (*middle*), and the image of the residuals (*bottom*) determined for the U band. This same procedure was applied to the B and V images after convolving them to have the same PSF as the U band. Each band was fitted with ELLIPSE separately but with the same mask and fixed values for the galaxy center, position angle, and ellipticity.

The resulting model disk component is characterized by a scale length of 2.7 kpc in all three filters, about 30% smaller than the average R_0 computed in § 3 from the original images (disk + star-forming regions). Its mean colors are $(B - V) \simeq 0.5$ and $(U - B) \simeq -0.2$ mag, which correspond to an age of about 1 Gyr and 200 Myr, respectively, according to a SSP synthesized with Starburst99 for an SMC-like metallicity. These values are consistent with the ages derived from the color profiles for $R < 4$ kpc; therefore, subtracting the model disk component is equivalent to removing the light from the diffuse stellar populations older than $\sim$100 Myr. The model disk component makes up about 27%, 36%, and 42% of the total light of the galaxy in the U, B, and V filters, respectively.

The observed $(U - B)$ and $(B - V)$ colors of the pixels in the residual images are plotted in Figure 5 as a function of distance from the galaxy center. These colors have been corrected only for Galactic extinction. The gray scale of the color distributions is based on a grid of two-dimensional bins, 0.4 kpc $\times$ 0.2 mag in size in $(U - B)$ and 0.4 kpc $\times$ 0.1 mag in size in $(B - V)$. We count the number of pixels falling into each bin and scale the gray shades by the maximum, so that the gray grows darker as the number of pixels increases. The y-axis on the right in both panels qualitatively links colors to stellar ages of a SSP synthesized with Starburst99 for an SMC-like metallicity (in units of 10^6 yr). We notice that the residuals within 2 kpc of the galaxy center are relatively redder and older than those at larger distances, while there is a significant blue (few Myr old) stellar population at galactocentric radii larger than 3–4 kpc.

In what follows, we restrict our analysis to the pixels in the residual images. Our aim is to estimate their stellar age and stellar mass surface density (§ 4.1), with which we will reconstruct the star formation history in IC 2574 in the last 10^8 yr (§ 4.2). We will compare the star formation activity of this galaxy with its H I properties to assess the applicability of the Schmidt law on local and global scales (§ 4.3). Finally, we will investigate the possible stellar origin of the H I holes detected in IC 2574 to examine the effects of stellar feedback on the ISM (§ 5).

4.1. *Age and Mass Estimates*

In order to assign an age and a mass density for each pixel in the residual images, we compare the observed photometry to

FIG. 4.—Example of how the smooth disk component is subtracted from the original images. The top panel shows the initial image, in this case the U frame; the middle panel shows the model disk component obtained with ELLIPSE after having masked those regions in IC 2574 bluer than $(U - B) = -0.3$ mag and with a S/N larger than 5 in all filters (*white areas*). Finally, the bottom panel shows the residuals after subtracting this model from the original U image. Flux increases as the gray shade becomes darker. All images are oriented so that north is up and east is to the left; their size is 15 $\times$ 11 kpc.

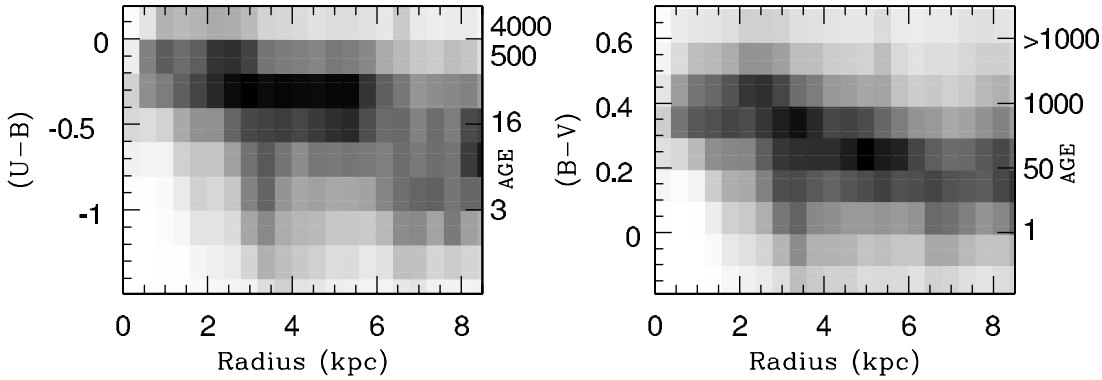

FIG. 5.—Radial distribution of observed $(U - B)$ and $(B - V)$ colors in the residual images (after subtracting the smooth disk model), corrected only for Galactic extinction. The gray scale indicates the number of pixels in each bidimensional bin [0.4 kpc $\times$ 0.2(0.1) mag for $(U - B)$ and $(B - V)$]; it gets darker as the number of pixels increases. In both panels the right y-axis shows the stellar ages corresponding to the colors on the left y-axis. These stellar ages are in units of 10^6 yr and refer to a SSP computed with Starburst99 for an SMC-like metallicity.

synthetic stellar populations convolved with a specific reddening law. We run Starburst99 to compute the colors of an instantaneous starburst (SSP) with a total mass of $10^6\ M_\odot$ as a function of its age. For this purpose, we adopt the default parameters of Starburst99, except for the metallicity, which we choose to be SMC-like following Stewart & Walter (2000). We assume a multipower law for the initial mass function (IMF) to approximate a Kroupa (2001) IMF, with an exponent of 1.3 for stars in the range 0.1–0.5 $M_\odot$ and 2.3 for the interval 0.5–100 $M_\odot$. Only stars with masses between 8 and 120 $M_\odot$ produce supernovae. Stellar winds and mass loss are computed with the theoretical model, which solves for the radiative transfer and the momentum equation in the stellar wind (see Leitherer et al. 1992). Finally, we use the Geneva evolutionary tracks with high mass loss; as discussed by Meynet et al. (1994), these tracks better reproduce the low luminosity observed for some WR stars, the surface chemical composition of WC and WO stars, and the ratio of blue to red supergiants in the star clusters in the Magellanic Clouds. The choice of an instantaneous starburst may be an oversimplified approach to the study of a star formation history that is expected to be more complicated in reality. On the other hand, our analysis is restricted only to star-forming regions younger than 10^8 yr, and this short time interval can be represented with an instantaneous starburst reasonably well.

We select all pixels in the residual images with a S/N larger than 5 in all filters and with a U-band flux 5 σ above the background level. We compare their colors (corrected for Galactic extinction) with the synthetic colors of Starburst99 using the technique described in Pasquali et al. (2003). Briefly, the synthetic colors of a SSP are reddened according to a preselected extinction law by a quantity $E(B - V)_i$, which is a free parameter varying across a predefined interval. This parameter represents the dust obscuration within the galaxy itself, and we refer to it as "intrinsic reddening." For a given $E(B - V)_i$, a χ^2 is calculated as the sum of the differences between the observed and reddened synthetic colors, normalized by the observational errors. Its minimum value, $\chi^2_{\rm min}$, establishes the best-fitting age, intrinsic reddening, and reddened synthetic magnitudes in the U, B, and V bands. The stellar mass enclosed in each pixel is then determined via the scaling relation

$$M_{\rm pix} = 10^{-0.4(m_{\rm obs} - m_{\rm syn})} \times 10^6\ M_\odot.$$

We compute $M_{\rm pix}$ in U, B, and V and take the mean of these three values.

Although at mid-IR wavelengths the intrinsic reddening of IC 2574 is negligible (see Cannon et al. 2005; Dale et al. 2007), at optical wavelengths it appears to be more prominent. Miller & Hodge (1994) performed optical spectroscopy of the northeast complex of H II regions and measured an intrinsic reddening of the gas, $E(B - V)_i^{\rm gas}$, between 0.3 and 0.5 mag, which translates into a stellar $E(B - V)_i$ of 0.13–0.22 mag (see Calzetti 2001). More recently, J. Moustakas et al. (2008, in preparation) derived $E(B - V)_i^{\rm gas} \simeq 0.15$ mag over an aperture of 10″ in radius at the center of IC 2574, which implies even lower stellar $E(B - V)_i$. Therefore, we decide to restrict the range of values available for $E(B - V)_i$ in our fitting procedure between 0.0 and 0.13 mag and to apply reddening with the extinction law derived for the SMC by Bouchet et al. (1985). We also use our dating technique in the assumption of a reddening-free environment [imposing $E(B - V)_i = 0.0$ everywhere in the galaxy] to check for systematic effects on the output ages and mass densities due to our specific treatment of dust obscuration.

In the dating technique of Pasquali et al. (2003), the errors on each best-fitting parameter are given by the minimum and maximum value of that parameter among all the fits which realize $\chi^2 < 1.5\chi^2_{\rm min}$ (corresponding to about 2 σ). In the case of IC 2574 we compute an average uncertainty of a factor of 2 on age, reddening, and mass.

4.2. *The Spatial Distribution of Stellar Ages and Mass Densities*

The distribution of stellar ages (obtained by correcting for intrinsic reddening) across the residual images is shown in Figure 6. The left panel plots the distribution of pixel stellar ages as a function of pixel galactocentric distance with the help of a gray scale, which indicates the number of pixels in each two-dimensional bin, 0.4 dex in age times 0.4 kpc in radius. The gray shade gets darker with increasing numbers of pixels. The contours (tracing equal numbers of pixels across the bins) highlight two major epochs of star formation in IC 2574. The older burst occurred about 100 Myr ago within $R < 4$ kpc of the center, while the second event took place between 10 and 1 Myr ago, mostly at $R \geq 4$ kpc. Star formation proceeded in between the two bursts, but with a somewhat lower rate. Globally, the stellar ages decrease with increasing distance from the galaxy center.

The age histograms for all pixels at a galactocentric distance smaller and larger than 4 kpc are traced in Figure 6 (*right*) with black and gray lines, respectively. Both histograms are normalized by the total number of pixels from which they are derived. If

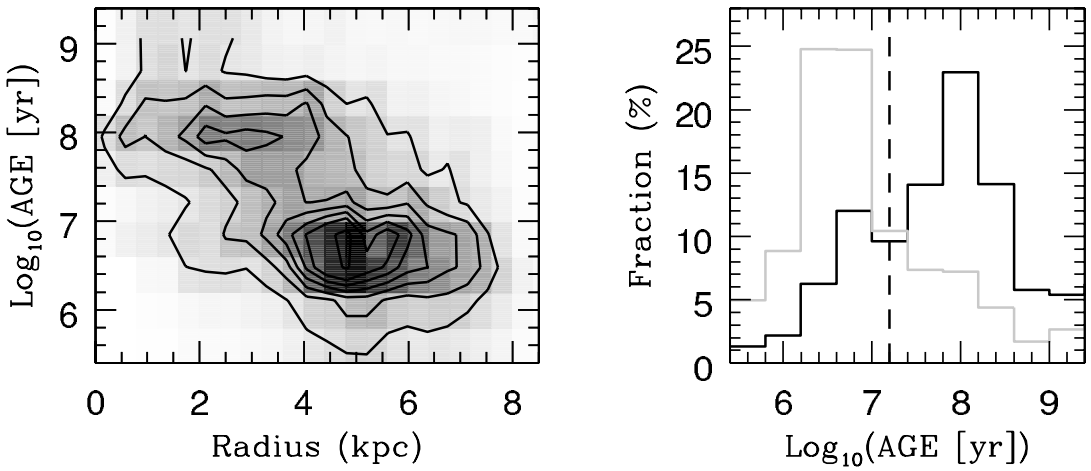

FIG. 6.—Luminosity-weighted age distribution of the stellar populations across IC 2574, obtained from the residual images after correction for reddening. The left panel shows the distribution of pixel stellar age as a function of pixel galactocentric distance. The gray scale indicates the number of pixels in each two-dimensional bin, 0.4 dex $\times$ 0.4 kpc in size. The gray shade becomes darker with an increasing number of pixels. The black lines are simply the contours drawn per constant number of pixels, with the following levels: 0.5, 1, 1.5, 2, 2.5, 3, 4, and 5×10^4. The right panel plots the age histogram for all pixels with $R < 4$ kpc (*black line*) and $R \geq 4$ kpc (*gray line*). Both histograms are normalized by the total number of pixels within and outside 4 kpc, respectively. The dashed line corresponds to $\log_{10}(\mathrm{age}) = 7.2$(16 Myr), the value we use to separate the younger from the older burst.

we assume a value of 16 Myr [$\log_{10}(\mathrm{age}) = 7.2$] to discriminate between the younger and older burst, we can estimate the spatial coverage of the two bursts in the inner and outer disks of IC 2574. For galactocentric distances smaller than 4 kpc, the older burst occurred over 73% of the pixels, while the younger one involved only 27% of the area. In the outer regions, instead, the younger burst lit up 70% of the pixels, and the older burst took place only in 30% of the area.

Repeating the same analysis but switching off the reddening correction confirms these trends. The younger and older bursts are still prominent and well defined, and they turn out to have similar timescales as determined when reddening is applied. Only the spatial coverage of the two bursts varies, and this only by 5% at most.

The distribution of the stellar mass surface densities (obtained including the correction for intrinsic reddening) as a function of galactocentric distance is presented in Figure 7 for the younger burst (*left*) and the older burst (*right*). Here the gray scale indicates the number of pixels in each two-dimensional bin, 0.4 dex $\times$ 0.4 kpc in size. The contours, which trace equal numbers of pixels across the bins, are computed for all the pixels with no age selection and are the same in both panels. All stellar mass surface densities are corrected for inclination. We can see that the older burst involves stellar mass surface densities larger than $\sim$0.2 $M_\odot$ pc^{-2} and has a characteristic stellar mass surface density of about 1 $M_\odot$ pc^{-2}. The younger burst is instead associated with stellar mass surface densities lower than 0.2 $M_\odot$ pc^{-2} with a characteristic value of about 0.04 $M_\odot$ pc^{-2}. The stellar mass surface density contours trace a radial profile which follows an exponential disk with a scale length of about 2.7 kpc and a central mass density of $\sim$5 $M_\odot$ pc^{-2}.

Correcting for reddening yields lower ages and higher stellar luminosities, and hence larger stellar masses, than assuming no extinction. With the constraint that $E(B-V)_i$ is <0.13 mag (see § 4.1), we obtain mass surface densities that are up to 40% larger than those assuming $E(B-V)_i = 0.0$ everywhere. The assumption of $E(B-V)_i = 0.0$ everywhere in the galaxy results in a lower characteristic stellar mass surface density of about 0.6 and 0.03 $M_\odot$ pc^{-2} for the older and younger burst, respectively. It also

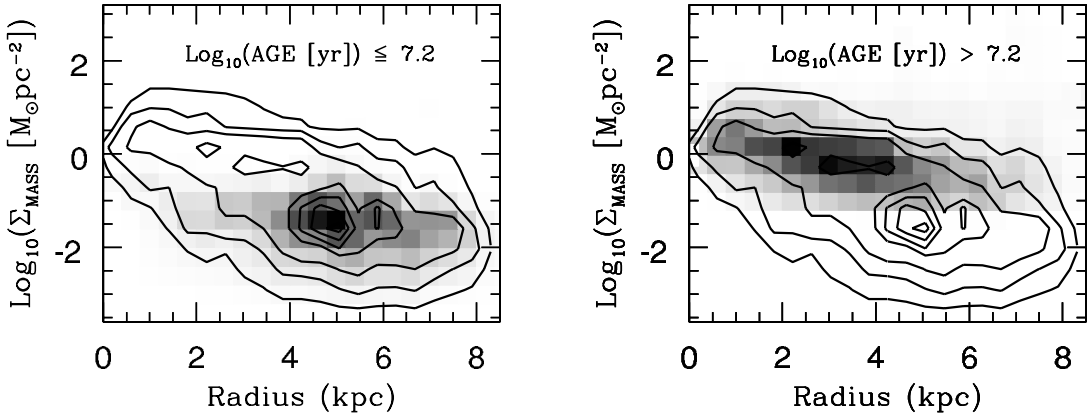

FIG. 7.—Stellar mass surface density distribution across IC 2574 obtained after correction for reddening. The left panel shows the distribution of the mass surface density produced by the younger burst, while the right panel shows the radial variation of the mass density obtained for the older burst. Once again, the gray scale indicates the number of pixels in each two-dimensional bin, 0.4 dex $\times$ 0.4 kpc in size. Its shade grows darker as the number of pixels increases. The black contours trace bins of equal numbers of pixels and are drawn with the following levels: 0.2, 0.5, 1, 2, 2.5, 3, 3.5, and 4×10^4 pixels. They have been computed for all the pixels with no age selection. All stellar mass surface densities have been corrected for inclination.

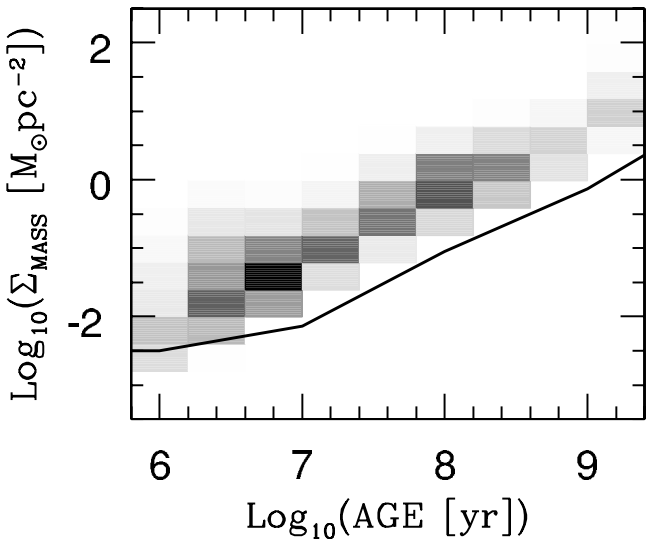

FIG. 8.—Distribution of stellar mass surface density (corrected for inclination) as a function of stellar age (obtained after correction for reddening). The gray scale is based on the number of pixels within each two-dimensional bin, 0.4 dex × 0.4 kpc in size, and it grows darker as this number increases. The solid line corresponds to a detection threshold of $3.2 \times 10^{-3}\ M_\odot\ \mathrm{pc}^{-2}$ or $0.12\ M_\odot\ \mathrm{pixel}^{-1}$.

gives a slightly larger scale length of 3 kpc and a central stellar mass surface density of $\sim 6\ M_\odot\ \mathrm{pc}^{-2}$.

Independent of the reddening, there is a relationship between age and mass surface density in our results, in the sense that older stellar ages are associated with higher stellar mass surface densities. This is shown in more detail in Figure 8, where the stellar mass surface density (corrected for inclination) is plotted as a function of age. The gray scale is based on the number of pixels within each two-dimensional bin, 0.4 dex × 0.4 kpc in size. The lower edge of the distribution is a selection effect created by requiring a *U*-band detection in order to carry out the analysis. Since older stars emit less *U*-band light, there must be more of them to reach the same surface brightness limit. The solid line in Figure 8 shows that the lower edge of the relationship matches our photometric detection threshold of 26 mag arcsec^{-2}, corresponding to a physical detection threshold of $3.2 \times 10^{-3}\ M_\odot\ \mathrm{pc}^{-2}$ or $0.12\ M_\odot\ \mathrm{pixel}^{-1}$. There is, however, no obstacle to detecting a stellar component younger than a few Myr and as massive as the older burst. The fact that such high stellar mass surface densities are not derived for the younger burst may hint at a constant SFR over the last 10^8 yr, so that the younger burst has not yet had time to build up all the stellar mass assembled by the older burst.

From all the pixels enclosed in an ellipse of semimajor axis $a = 8$ kpc and semiminor axis $b = 3.5$ kpc (P.A. = 55°) we derive a total mass of about $4.4 \times 10^7\ M_\odot$ for the stars younger than 1 Gyr (from the fits that include the reddening correction), of which $\simeq 3 \times 10^6\ M_\odot$ were produced during the younger burst and $\simeq 4.1 \times 10^7\ M_\odot$ during the older burst. Switching off the reddening correction in our dating technique gives lower values: a total mass of about $3.9 \times 10^7\ M_\odot$ split between $\simeq 2 \times 10^6$ and $\simeq 3.7 \times 10^7\ M_\odot$ for the younger and older burst, respectively.

Although a SSP based on the assumption of an instantaneous burst does not provide a true SFR, we can estimate one from the ratio of the total stellar mass produced during a burst to the mean stellar age of the same burst. This exercise is based on the pixel-by-pixel maps of stellar age and mass surface density computed by omitting the reddening correction, so that we can compare the results with the SFR derived in the literature from the galaxy observed Hα flux (i.e., not corrected for intrinsic reddening). Therefore, for a mean stellar age of $\simeq$4 and 150 Myr for the younger and older burst, respectively, and the burst total masses as listed above, we derive a SFR of about 0.5 and 0.2 $M_\odot\ \mathrm{yr}^{-1}$. Given that the typical uncertainty in our age and mass estimates is a factor of 2, the error on the SFR corresponds to about a factor of 3, and within this uncertainty we may infer that the SFR has been nearly constant over the last few 10^8 yr in IC 2574. For comparison, the SFR derived from the Hα flux by Miller & Hodge (1994) is $\simeq 0.1\ M_\odot\ \mathrm{yr}^{-1}$. This value suffers its own uncertainties concerning the depth of the observations, as well as the escape fraction of ionizing photons emitted by young and massive stars, which can be as high as 50% (see Weedman 1991; Pasquali & Castangia 2008).

As already noted in §§ 1 and 3, the northeast complex of H II regions, also associated with a H I supergiant shell, is the brightest site of star formation in IC 2574. In order to investigate whether its stellar populations are different from the rest of the galaxy, we analyze the distributions of pixel stellar ages and mass surface densities within the supergiant shell. These are plotted in Figure 9 as a function of distance from the shell center. Here each two-dimensional bin is 0.4 dex × 28 pc in size. The shell is spatially rather uniform in age, except perhaps for ages younger than 3 Myr [$\log_{10}(\mathrm{age}) = 6.5$], which show up only at radii larger than 400 pc. It appears that the most significant episode of star formation

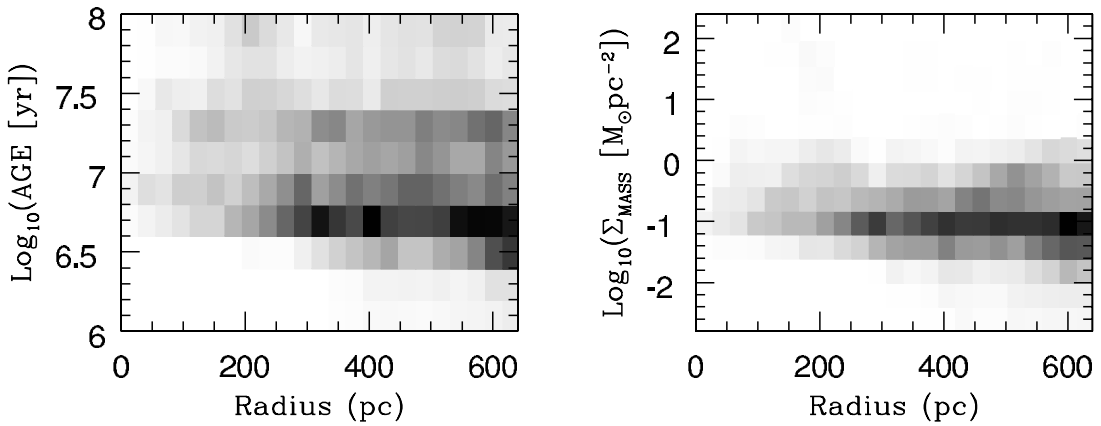

FIG. 9.—Distributions of pixel stellar age and mass surface density as a function of pixel distance from the center of the supergiant shell in the northeast complex of H II regions. Stellar mass surface densities are corrected for inclination. Stellar ages and mass surface densities are obtained from the fits which apply the correction for reddening.

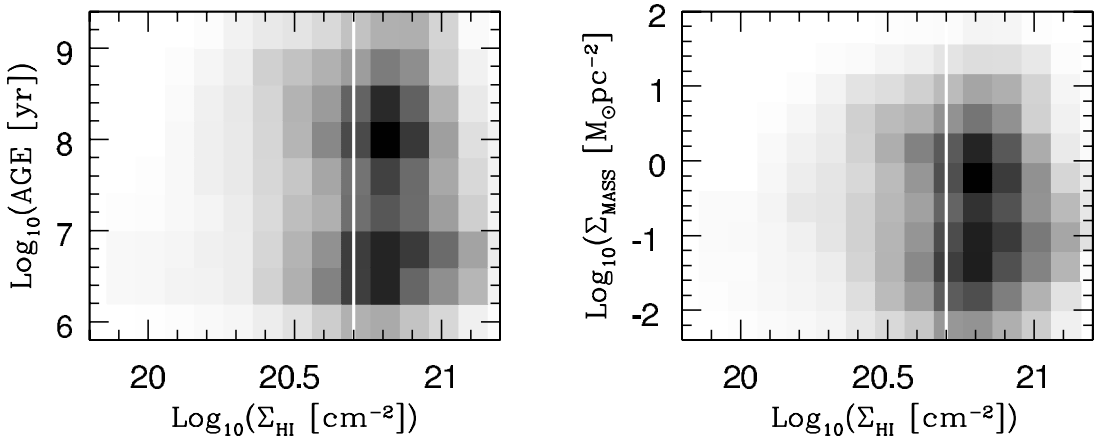

FIG. 10.—Pixel stellar ages and mass surface densities as a function of H I column density corrected for inclination. Each two-dimensional bin is 0.4×0.2 dex in size and is color-coded on the basis of the number of pixels falling within it. The gray shade becomes darker with an increasing number of pixels. The vertical line indicates the characteristic critical density obtained by Kennicutt (1989), $\sim 5 \times 10^{20}$ cm^{-2}.

occurred about 5 Myr ago; a previous burst may be identified in a more modest peak of the distribution at an age of ~20 Myr. As discussed by Walter et al. (1998) and Walter & Brinks (1999), the shell contains a star cluster and has nine star-forming regions distributed along its rim. Stewart & Walter (2000) estimated an age of 11 Myr for the star cluster and 3 Myr for the star-forming regions. From the LBT data we derive an age of about 5 Myr for the cluster and 1–3 Myr for the shell rim. These values do not change significantly when the correction for intrinsic reddening is omitted or the diffuse large-scale disk is not removed. The discrepancy in the cluster age between this work and Stewart & Walter could be related to different IMF and evolutionary tracks and to a different treatment of reddening, which can be quite patchy within the shell. However, given the factor of 2 uncertainties in our age estimates, these two results are consistent. The stellar mass surface density of the shell varies between 0.01 and 1 $M_\odot$ pc^{-2} and peaks at about 0.1 $M_\odot$ pc^{-2}.

4.3. *Comparison with the* H I *Column Density Map*

Figure 10 shows the distribution of pixel stellar ages and mass surface densities as a function of the H I column density corrected for inclination. Here each two-dimensional bin is 0.4×0.2 dex in size. No correlation arises from these plots, except for the fact that the star formation activity in IC 2574 seems to preferably occur in regions with $\Sigma_{\rm H\,I} \simeq 6 \times 10^{20}$ cm^{-2}. This value is comparable with the critical density derived by Skillman (1987; $\sim 10^{21}$ cm^{-2}) for a number of irregular galaxies and Kennicutt (1989; $\sim 5 \times 10^{20}$ cm^{-2}) for a sample of disk galaxies. Column densities smaller than $\sim 10^{20}$ cm^{-2} are measured in correspondence with H I holes and may not be representative of the local H I gas prior to the formation of the holes.

The lack of any correlation between star formation and H I gas on local scales was also observed in seven spiral galaxies by Wong & Blitz (2002), in NGC 6822 by de Blok & Walter (2006), in M51a by Kennicutt et al. (2007), and for a large galaxy sample by Bigiel et al. (2008). In the case of M51a, Kennicutt et al. showed that the local star formation density correlates with the local H_2 density (and thus the local H I + H_2 density). In IC 2574, we expect that most of the ISM is atomic, and we might expect a relationship between H I and SFR based on both formation of and feedback from young stars. From formation, the correlation observed between H_2 and SFR in gas-rich spirals might suggest that the gas reservoir, here probably H I, dictates the SFR. From feedback, we would expect a correlation if H I forms via photodissociation of H_2 powered by the stellar UV radiation field (Shaya & Federman 1987; Tilanus & Allen 1991; Allen et al. 1997) or an anticorrelation if the stellar radiation field ionizes H I into H II. None of these predictions appear to be borne out by the results seen in Figure 10. We are then led to conclude that there is no evidence in our data either that H I sets the SFR or that star formation creates or ionizes a significant fraction of H I.

5. STELLAR PROPERTIES OF THE H I HOLES

The lack of correlation between H I and star formation is especially striking in IC 2574, where the H I distribution is marked by a wealth of holes. A natural explanation for these structures is that they are carved out by feedback from star formation, but the lack of a correlation between atomic gas and the SFR calls such a relationship into question. In this section we ask whether young stars have been able to produce the observed H I holes and sustain their expansion; we also ask whether such holes are a natural consequence of the star formation we observe and investigate the implications of the lack of H I–SFR correlation for stellar feedback.

5.1. *Are the* H I *Holes Powered by Stars?*

Walter & Brinks (1999) identified 48 holes and measured their diameter, expansion velocity, dynamical age, volume/column density, and H I mass. These holes are long-lived features; since IC 2574 largely rotates as a solid body, the shear computed from its smoothed rotation curve turns out to disrupt the H I holes over timescales larger than 0.5 Gyr. Out of the initial 48 holes, only 15 are overlaid on the residual images of IC 2574 obtained after subtracting the smooth disk component (see § 4) and have a measured velocity expansion and more than 80% of their area filled with pixels carrying information on stellar age and mass density. Similar to the supergiant shell whose star cluster is off-center (Walter & Brinks 1999; Stewart & Walter 2000), we do not detect any central star cluster in these 15 H I holes, but rather a spatial mixture of populations formed during the younger and older bursts. The spatial distribution of the younger population within each H I hole can be clumpy, with the clumps often located at the periphery of the H I hole. Figure 11 shows the radial distribution of pixels with an associated stellar age younger than 16 Myr (corresponding to the younger burst) obtained for each H I hole. The three panels of Figure 11 distinguish the holes completely filled by young stellar populations (*left*) from those where young stellar ages are found in the periphery (*middle*) and those where young stellar populations

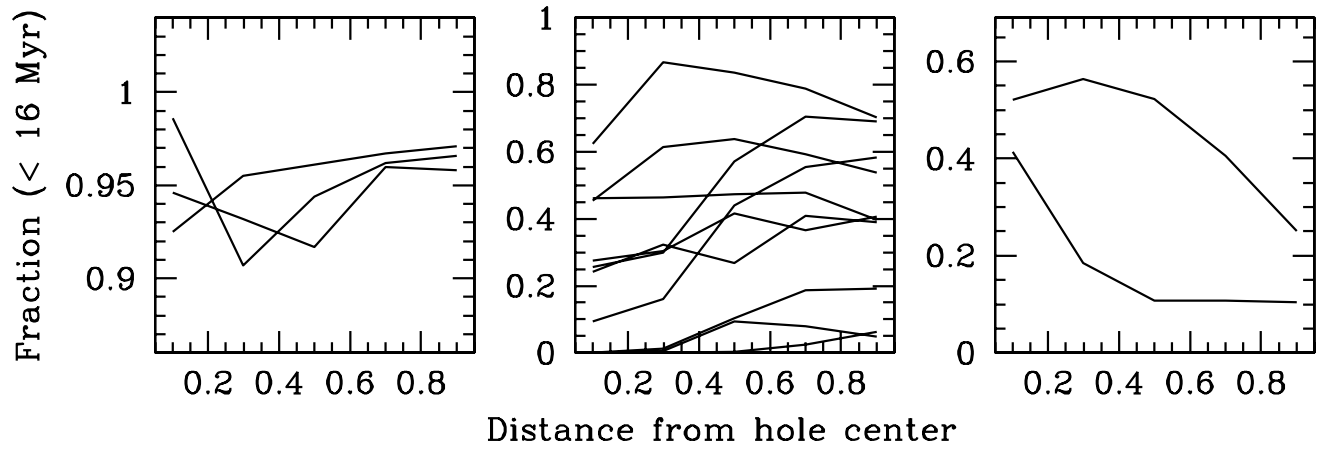

FIG. 11.—Fraction of pixels associated with a stellar age younger than 16 Myr as a function of distance from the hole center. The distance is in units of the respective hole radius. The number of "young" pixels per bin of distance is normalized by the total number of pixels younger than 16 Myr. *Left*: Holes filled with young stellar populations (3 of 15). *Middle*: Holes with young stellar populations along the outskirts (10 of 15). *Right*: Holes with centrally concentrated young stellar populations (2 of 15).

are preferentially central (*right*). We express the distance of each pixel from the hole center in units of the respective hole radius and compute the number of pixels younger than 16 Myr per distance bin, as well as the total number of pixels younger than 16 Myr within the hole. We use this latter quantity to normalize the former, and in this way we derive the fraction of "young" pixels as a function of distance within a H I hole. Apart from the three holes in the left panel that are completely dominated by a young stellar component, in most cases (including the supergiant shell) this young stellar population lives in the outskirts of a hole, at a distance larger than 0.4 times the hole radius (*middle*). Only in two holes does the young component look more centrally concentrated (*right*).

For these 15 holes we also estimate (1) the fraction of pixels associated with a stellar age younger than 16 Myr ($f_{\rm YOUNG}$), defined as the ratio of pixels associated with stellar ages younger than 16 Myr to the total number of pixels within a hole; (2) the mean age of the stellar populations produced during the younger burst (with an age <16 Myr); (3) the total stellar energy released by the stellar winds and supernova explosions of the young population ($E_{\rm YOUNG}$); and, finally, (4) the kinetic energy of the H I holes in terms of a fraction of the total energy provided by their young stellar populations. We compute the stellar total energy, $E_{\rm YOUNG}$, from the value derived by Starburst99 at the mean age of the young component within a hole and properly scaled by its total mass. The kinetic energy of a hole is determined from its column density corrected for inclination ($\Sigma_{\rm H\,I}$ estimated by Walter & Brinks) and its expansion velocity ($V_{\rm exp}$), $E_{\rm H\,I} = 0.5\Sigma_{\rm H\,I}({\rm area})V_{\rm exp}^2$, where "area" is the area of the hole whose diameter is listed in Walter & Brinks. We then calculate the ratio of the hole kinetic energy to the stellar total energy, $E_{\rm H\,I}/E_{\rm YOUNG}$; this ratio is a measure of the efficiency at which the total stellar energy is transformed into the kinetic energy of the H I gas.

All the parameters mentioned above are plotted in Figure 12. Figure 12*a* presents $f_{\rm YOUNG}$ as a function of the hole diameter in parsecs. No correlation is seen between these two parameters. The mean age of the young stellar component is plotted as a function of the hole dynamical age in Figure 12*b*. Here there is a hint of a relation in which both the young component and the hole age together, although the stars generally appear to be younger than their associated hole by a factor of 5, on average. We note here that the dynamical age of the holes is an upper limit to the true hole age, since Walter & Brinks (1999) derived the dynamical age under the assumption of a constant expansion velocity, while these holes have certainly expanded faster in the past. Because of the uncertainty of this assumption and the errors in our dating technique, it is difficult to establish how much older (if at all) the H I holes are compared to their young stellar component. As shown in Figure 12*c*, the total energy released by the young stellar component is typically an order of magnitude larger than the kinetic energy of the H I holes and lies above the one-to-one correspondence (*gray line*). Indeed, the ratio of the hole kinetic energy to the total stellar energy is, on average, about 10%, thus indicating that hole expansion can be sustained with only 10% of the available total stellar energy (see Fig. 12*d*). This overall picture does not qualitatively change when we use the stellar populations obtained by switching off the reddening correction in our dating technique. In this case, the ratio of the hole kinetic energy to the total stellar energy increases from 10% to about 20%, since the output stellar mass surface density is lower when reddening is neglected. An $E_{\rm H\,I}/E_{\rm YOUNG}$ ratio of $\sim$10%–20% is in agreement with the value (10%–20%) independently obtained by Cole et al. (1994) from modeling the galaxy luminosity function, while Bradamante et al. (1998) determined a value of 3% for supernovae Type II and 100% for supernovae Type Ia from the modeling of the chemical evolution of blue compact galaxies.

5.2. *Why Is It that Not All Star Formation Creates Holes?*

If a conclusion from Figure 12 is that the stellar energy budget is, in principle, large enough to support hole expansion, we may then ask why many star-forming regions in IC 2574 are not located in H I holes. We build a sample of 105 control apertures with the diameter (7″, or 136 pc at the assumed distance of IC 2574) of the beam of the H I observations, placed randomly across the galaxy to sample different stellar populations and different values of the H I column density away from the observed H I holes. For each aperture, we measure $f_{\rm YOUNG}$, $E_{\rm YOUNG}$, $\Sigma_{\rm H\,I}$, the average H I velocity dispersion, $\sigma_{\rm H\,I}$ (from the H I second moment map of Walter & Brinks 1999), $E_{\rm H\,I}$ defined as $1.5\Sigma_{\rm H\,I}({\rm area})\sigma_{\rm H\,I}^2$ (where area is the area of the apertures), and the energy ratio $E_{\rm H\,I}/E_{\rm YOUNG}$. All these properties are plotted in gray in Figure 13 for only those 37 apertures with $f_{\rm YOUNG} > 70\%$, so that their stellar populations mostly formed during the younger burst. In black are the observed 15 H I holes, whose $\sigma_{\rm H\,I}$ we measure in an annulus about 100 pc wide around each hole and whose $\Sigma_{\rm H\,I}$ was estimated by Walter & Brinks. The assumption here is that the H I properties outside a H I hole may be representative of the local gas before the hole formation. Figure 13*a* shows the total stellar energy $E_{\rm YOUNG}$ as a function

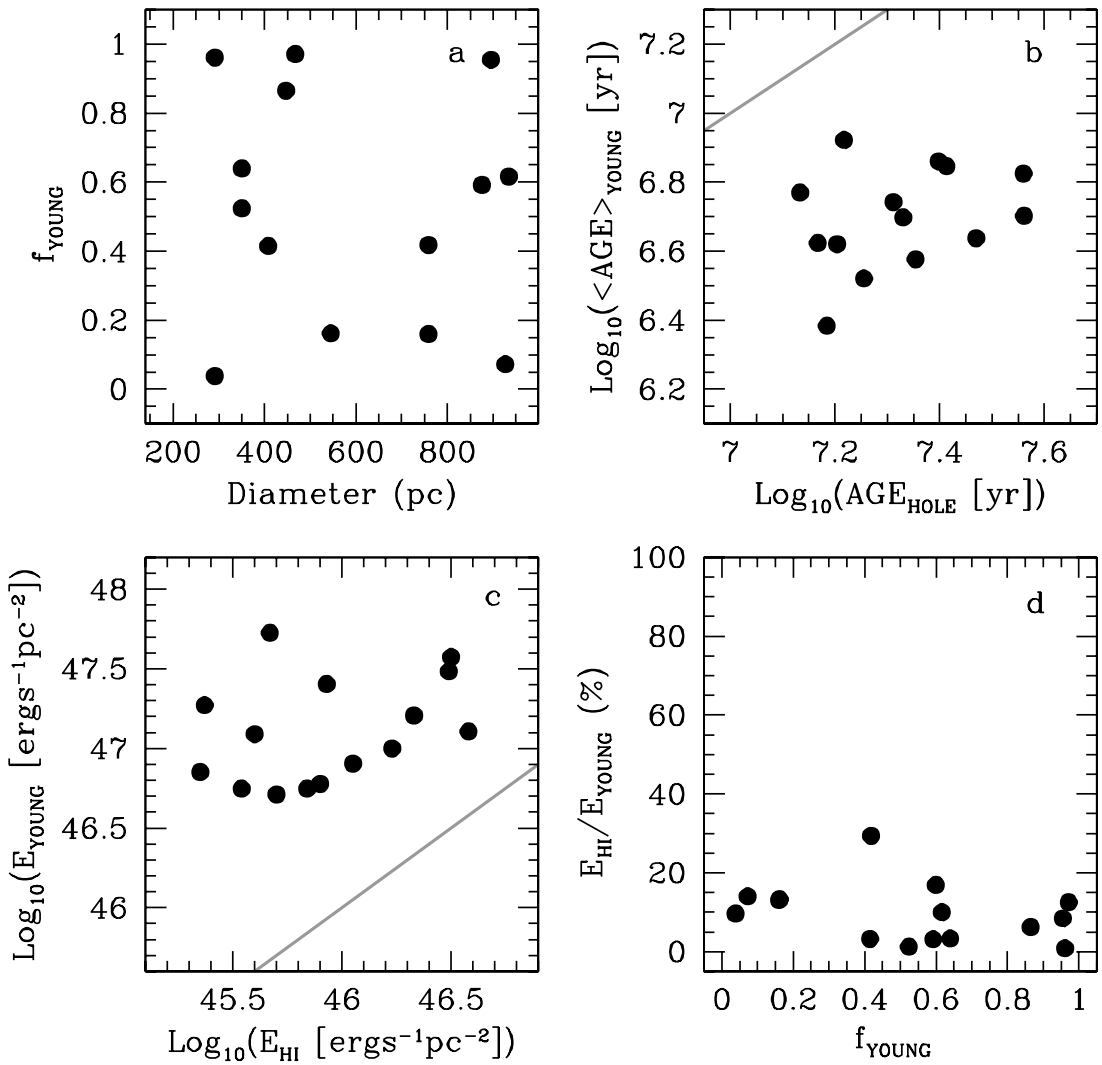

FIG. 12.—Total energy budget of the younger burst (<16 Myr) detected within 15 H I holes. (*a*) Ratio of pixels associated with stellar ages younger than 16 Myr to the total number of pixels within a hole plotted as a function of hole diameter in parsecs. (*b*) Mean age of the young stellar component (<16 Myr) enclosed in a H I hole shown as a function of the hole dynamical age, simply computed from its diameter and expansion velocity. The holes' stellar and dynamical ages become equal along the gray line. (*c*) Total energy released by the stellar winds and supernova explosions of the young component traced as a function of the hole kinetic energy, derived from the hole expansion velocity. Both quantities are normalized by the hole area. The gray line indicates when the total stellar energy equals the hole kinetic energy. (*d*) Based on (*c*), the ratio of the hole kinetic energy to the total energy of its young component vs. the fraction of pixels associated with stellar ages <16 Myr.

of the H I kinetic energy, both parameters normalized by the area of the apertures (*gray circles*) and H I holes (*black circles*). The gray line indicates the one-to-one correspondence between these two energy terms. For the majority of apertures, as well as for all the H I holes, the total stellar energy is up to an order of magnitude larger than the H I kinetic energy. Indeed, the $E_{\rm H\,I}/E_{\rm YOUNG}$ ratio is lower than unity for about 70% of the control apertures, and the average $E_{\rm H\,I}/E_{\rm YOUNG}$ is $\simeq$35%, indicating that about one-third of the total stellar energy can account for the observed H I kinetic energy (see Fig. 13*b*). Yet no hole in the atomic H gas is detected at the position of these apertures. We notice that the apertures whose $E_{\rm H\,I}/E_{\rm YOUNG}$ is larger than 100% are systematically associated with $\Sigma_{\rm H\,I} \geq 8 \times 10^{20}$ cm^{-2}, i.e., high H I columns. The energy ratio for the H I holes is well below 100%, with an average value of about 10%; all H I holes have $\Sigma_{\rm H\,I} < 8 \times 10^{20}$ cm^{-2}. In Figure 13*c* the total stellar energy is compared with the average velocity dispersion for both the control apertures (*gray circles*) and the observed 15 H I holes (*black circles*). No clear correlation exists between these two parameters, although one could attempt to see $E_{\rm YOUNG}$ increasing with $\sigma_{\rm H\,I}$. This trend is also seen across a large sample of galaxies by Tamburro (2008) and could be interpreted as due to star formation inducing turbulence in the H I gas (see also Dib et al. 2006). The total stellar energy is plotted as a function of the H I column density, $\Sigma_{\rm H\,I}$, in Figure 13*d*; once again, no tight correlation can be seen in this plot, except perhaps for a weak trend whereby $E_{\rm YOUNG}$ decreases at larger $\Sigma_{\rm H\,I}$.

As pointed out by Walter & Brinks (1999), the H I velocity contours of IC 2574 are characterized by distortions due to noncircular motions. Noncircularity is believed to arise from star formation processes or from the presence of a bar, a spiral density wave, or noncircular halo potentials. Oh et al. (2008) have recently isolated the noncircular motions in IC 2574 and showed that their typical velocity is a few km s^{-1}, with peaks of $\sim$20 km s^{-1}. We use the map of the kinetic energy associated with noncircular motions constructed by Oh et al. ($E_{\rm H\,I}^{\rm ncir} = 0.5 M_{\rm ncir} V_{\rm ncir}^2$, where $M_{\rm ncir}$ is the H I mass associated with noncircular motion; see Oh et al. [2008] for further details) and compute the total kinetic energy in noncircular motions in the control apertures with $f_{\rm YOUNG} >$ 70%, as well as in the H I holes. We compare this energy with the

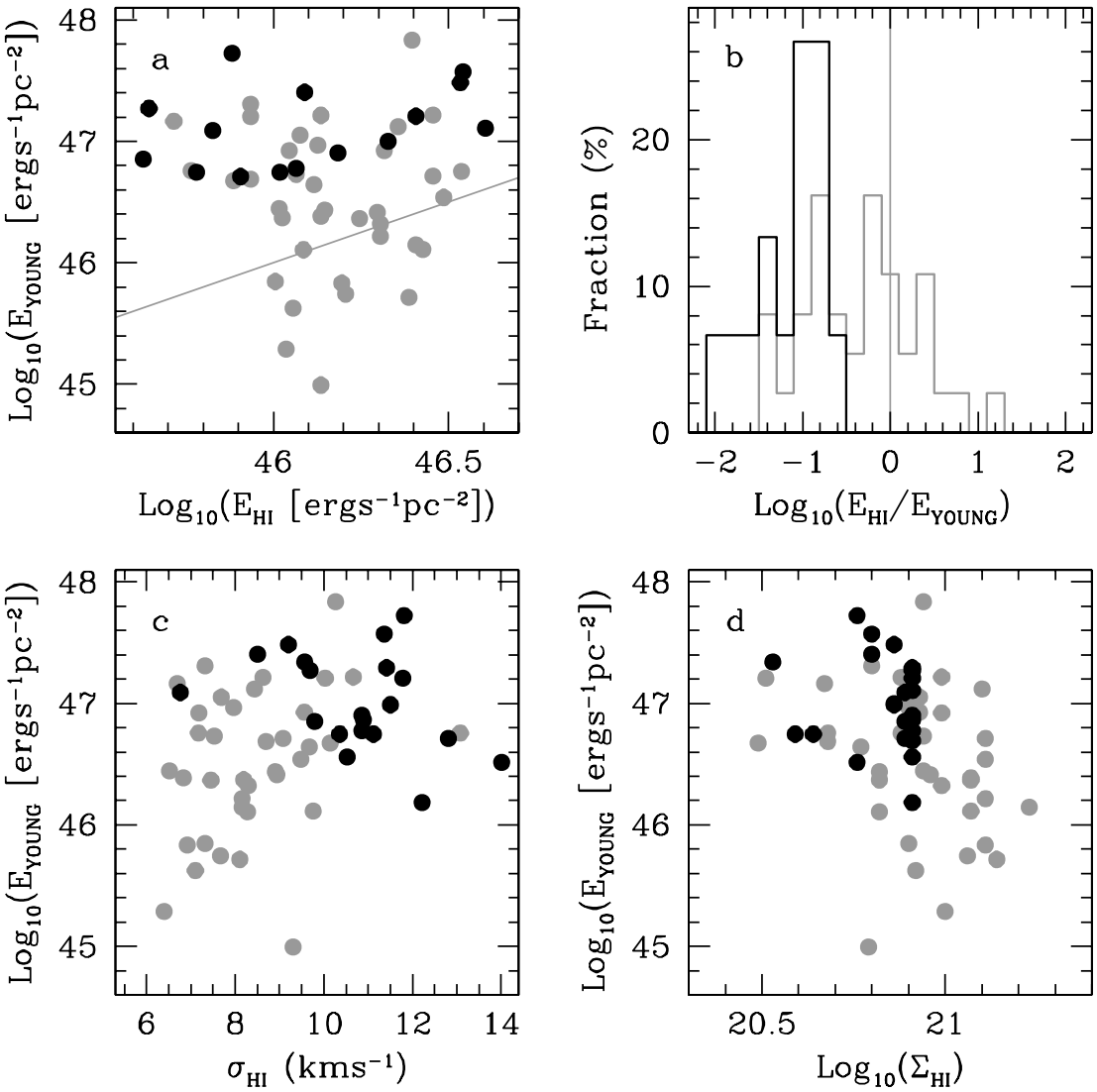

FIG. 13.—(*a*) Comparison of the total energy released by the stellar populations younger than 16 Myr with the H I kinetic energy based on the velocity dispersion of the atomic H gas. Black and gray circles represent 15 H I holes and control apertures, respectively. The latter are characterized by a fraction of pixels associated with stellar ages $\leq$16 Myr larger than 70%. The gray line indicates the one-to-one correspondence between $E_{\rm YOUNG}$ and $E_{\rm H\,I}$. Both energy terms are normalized by the area of the holes and the control apertures. (*b*) Distribution of the energy ratio $E_{\rm H\,I}/E_{\rm YOUNG}$, in black for the H I holes and in gray for the control apertures. The vertical gray line highlights the $E_{\rm H\,I}/E_{\rm YOUNG}$ value of 100%. (*c*) $E_{\rm YOUNG}$ as a function of the H I velocity dispersion, $\sigma_{\rm H\,I}$. (*d*) $E_{\rm YOUNG}$ as a function of the H I column density, $\Sigma_{\rm H\,I}$.

total stellar energy in Figure 14 (*left*), where the black and gray circles represent the H I holes and the control apertures, respectively, and the gray line traces the one-to-one correspondence between the kinetic noncircular and stellar energies. The large majority of control apertures and holes are placed above this line, indicating that the energy released by their young stellar population is larger than the kinetic energy of the in situ noncircular motions. The distribution of the control apertures (*gray line*) and holes (*black line*) in the energy ratio $E^{\rm ncir}_{\rm H\,I}/E_{\rm YOUNG}$ is plotted in Figure 14 (*right*). Values of $\log_{10}(E^{\rm ncir}_{\rm H\,I}/E_{\rm YOUNG}) < 0$ are obtained for those control apertures and holes where the total stellar energy is in excess of $E^{\rm ncir}_{\rm H\,I}$; they define an average $\langle E^{\rm ncir}_{\rm H\,I}/E_{\rm YOUNG}\rangle = 21\%$ (control apertures) and 43% (holes).

5.3. *Photoionization of* H I

There is a final aspect to consider in our analysis of H I hole formation, i.e., the ionization of the H I gas due to stellar radiation. So far, we have considered the total energy produced by the stellar winds and supernova explosions of the stellar population younger than 16 Myr. Figures 12 and 13 do not show any firm evidence for a stellar origin of the holes, although the H I kinetic energy of the holes and the control apertures is typically about 10%–30% of the total stellar energy. We now ask whether the H I holes are produced by the stellar radiation field via ionization of the atomic H gas. We estimate the number of ionizing photons, Q(H), in each hole and the control aperture from the value tabulated by Starburst99 at the age of the young component in the hole/aperture scaled by its total mass. We then use Q(H) to compute the radius, $R_{\rm S}$, of the Strömgren sphere associated with each H I hole and control aperture. The Strömgren sphere defines the volume within which all the H I gas is ionized, and its radius $R_{\rm S}$ is expressed by the equation $Q({\rm H}) = (4\pi R_{\rm S}^3 n_{\rm H\,I}^2 \alpha_B)/3$, where $n_{\rm H\,I}$ is the H I volume density and α_B is a scaling parameter depending on the gas temperature. From Osterbrock (1989) we assume $\alpha_B = 4.54 \times 10^{-13}$ for a gas temperature of 5000 K. We derive the H I volume density $n_{\rm H\,I}$ from the relation $\Sigma_{\rm H\,I} = (2\pi)^{1/2} h n_{\rm H\,I}$, where h, the scale height of the H I disk, is 440 pc as obtained by Walter & Brinks (1999) for a distance of 4.02 Mpc.

If all the stellar photons produced within the control apertures ionized the surrounding H I gas, the radius of the Strömgren

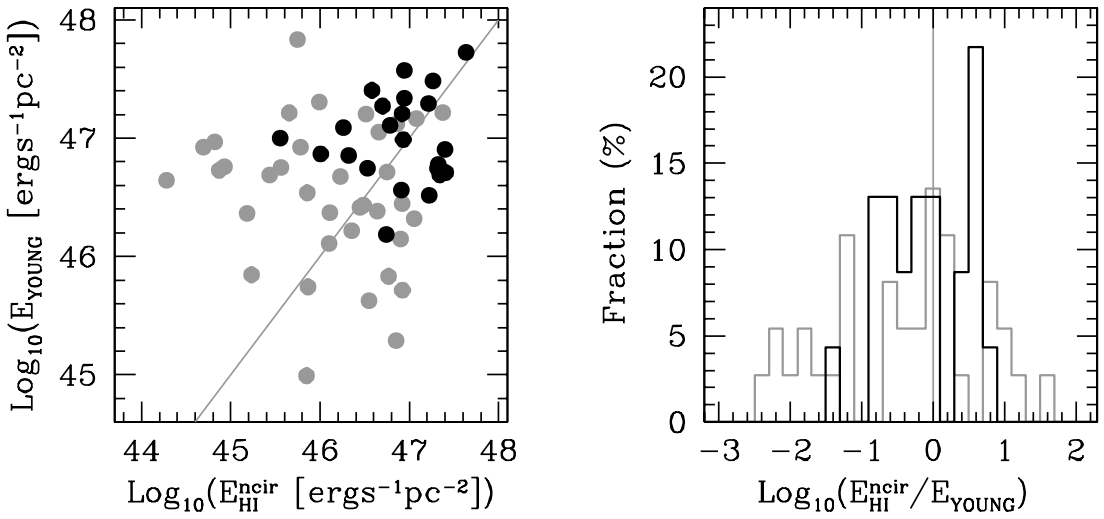

FIG. 14.—*Left*: Comparison of the total energy released by the stellar populations younger than 16 Myr, $E_{\rm YOUNG}$, and the H I kinetic energy associated with noncircular motions, $E_{\rm H\,I}^{\rm ncir}$. Black and gray circles represent the H I holes and the control apertures, respectively. *Right*: Distribution of the control apertures (*gray line*) and H I holes (*black line*) in the energy ratio $E_{\rm H\,I}^{\rm ncir}/E_{\rm YOUNG}$. The gray vertical line indicates $\log_{10}(E_{\rm H\,I}^{\rm ncir}/E_{\rm YOUNG}) = 0$, i.e., $E_{\rm H\,I}^{\rm ncir}/E_{\rm YOUNG} = 100\%$.

sphere of the control apertures with $f_{\rm YOUNG} > 70\%$ would be on average 4 times bigger than the aperture radius, and the apertures would lie in holes that are well observable. Given that the control apertures are not associated with H I holes by definition, only a much lower fraction of Q(H) can ionize the H I gas. This limits the number of ionizing photons to less than 20% of Q(H); under this assumption, the ratio of $R_{\rm S}$ to the aperture radius decreases to an average value of 2, consistent with an uncertainty on Q(H) of a factor of 3, which is due to the errors on the stellar ages and masses. This constraint would make any H I hole formed via ionization less likely to be detectable. For the H I holes with $f_{\rm YOUNG} > 70\%$, the UV radiation from the young stellar populations would produce a Strömgren sphere 4 times larger than the hole radius if 100% of the ionizing photons were available. Making the observed hole consistent with the Strömgren radius requires only $\sim$20% of the available photons. Therefore, such a limit on Q(H) may be sufficient to explain both the existence of those H I holes whose stellar populations are predominantly young (<16 Myr) and the lack of observable H I holes around the control apertures.

6. DISCUSSION AND CONCLUSIONS

Deep, LBT imaging in the U, B, and V bands has allowed us to spatially map the star formation history of IC 2574 over the last 10^8 yr. We do this by analyzing the pixel-by-pixel colors of all areas in IC 2574 with significant detections in all bands. Overall, the angle-averaged surface brightness profiles indicate a predominance of blue colors [$(U-B) < -0.3$ and $(B-V) < 0.4$ mag] at galactocentric radii larger than 4 kpc, mostly due to the presence of the large northeast complex of H II regions (associated with a H I supergiant shell) and the southwest extended tail of star formation. At a limiting brightness of 26 mag arcsec^{-2}, the major axes of the H I and U-band light distributions are nearly the same, while the minor axes are smaller in the optical. This could be due to differences in the scale height of the U-band light and H I distributions.

Using the dating technique of Pasquali et al. (2003), we are able to construct pixel-by-pixel maps of stellar age and mass surface density from the comparison of the observed colors with simple stellar population models synthesized with Starburst99. After fitting and subtracting a smooth disk component (whose colors point to a stellar age >200 Myr), our best-fitting Starburst99 models indicate the occurrence of two major bursts, one about 100 Myr ago and the other during the last 10 Myr. The older burst appears to be spatially "confined" within the inner 4 kpc (in galactocentric radius), while the younger episode of star formation occupies the 4 kpc $< R <$ 8 kpc region. The two episodes also differ in the stellar mass surface density of stars formed; the typical mass density associated with the older burst is about 1 $M_\odot$ pc^{-2}, while it is $\simeq$0.04 $M_\odot$ pc^{-2} for the younger burst. However, these values are luminosity-weighted and therefore biased. Given that the U-band flux emitted by a SSP decreases for increasing age, and the flux itself is proportional to the stars' total mass, the detection of stars above a fixed threshold in the U band (used in this study as a prior) requires stellar populations that are progressively more massive as they grow older. Quantitatively speaking, a limiting surface brightness of 26 mag arcsec^{-2} allows us to detect stellar populations older than 10^8 yr with a mass surface density larger than 0.1 $M_\odot$ pc^{-2}, while those populations a few Myr younger are detected down to a mass surface density of 0.003 $M_\odot$ pc^{-2} (a factor of $\sim$30 lower than at 100 Myr). The fact that we do not detect young stellar populations as massive as 1 $M_\odot$ pc^{-2} is not a selection effect of the data; it possibly hints at a constant SFR, at least over the last 10^8 yr, so that the younger burst has not yet had time to produce the same amount of stellar mass as was assembled during the older burst.

We compare both the stellar ages and the mass surface densities of the recently formed populations with the H I column density across IC 2574 and do not find any significant correlation between star formation activity and the H I reservoir in this galaxy. A similar result was obtained by Wong & Blitz (2002), de Blok & Walter (2006), Kennicutt et al. (2007), and Bigiel et al. (2008), using different tracers of star formation. The lack of any correlation between star formation and H I is in contrast to the expectation of a relationship between H I and SFR based on both formation of and feedback from young stars. In terms of star formation, the correlation observed between H_2 and SFR in gas-rich spirals might indicate that the H I gas reservoir controls the SFR. In terms of stellar feedback, instead, we would expect to see a correlation if H I forms via photodissociation of H_2 powered by the stellar UV radiation field (Shaya & Federman 1987; Tilanus & Allen 1991; Allen et al. 1997) or an anticorrelation if the stellar radiation field ionizes H I into H II. We thus conclude that star formation in IC 2574 is not regulated by the available H I gas reservoir, not efficient at creating H I via photodissociation, or actively

expelling or ionizing a significant fraction of the H I. On a global scale, star formation in IC 2574 appears to preferentially take place in regions where the H I column density is about 6×10^{20} cm^{-2}. This value is comparable with the global critical density derived by Skillman (1987; $\sim 10^{21}$ cm^{-2}) for a sample of irregular galaxies, by Kennicutt (1989; about 5×10^{20} cm^{-2}) for 33 disk galaxies, and by de Blok & Walter (2006) for NGC 6822 (5.6×10^{20} cm^{-2}) and with the theoretical values computed by Schaye (2004).

The lack of correlation between star formation activity and the H I density in IC 2574 is rather puzzling with respect to the distinct H I holes, as one would expect to systematically detect a central cluster of young stars driving the hole expansion through their stellar winds and supernova explosions. With the possible exception of the supergiant shell (see Stewart & Walter 2000), we do not observe any concentration of young stellar populations at the center of the H I holes, but rather a mixture of populations formed during the younger and older bursts, with the younger population often in clumps located at the periphery of the H I hole. We determine the fraction of pixels with a stellar age younger than 16 Myr ($f_{\rm YOUNG}$) for 15 of the 48 holes identified by Walter & Brinks (1999; i.e., those that overlap with the area of the galaxy obtained after the removal of its smooth disk component; see § 4). Here the age of 16 Myr is assumed to separate the younger from the older star formation episode identified by us. We also compute the mean age ($\langle {\rm age} \rangle_{\rm YOUNG}$) and the total energy ($E_{\rm YOUNG}$, due to stellar winds and supernova explosions) of the stars formed during the younger burst in each hole and compare them with the dynamical age and kinetic energy of the hole (based on its expansion velocity). The relevant results of such a comparison are as follows:

1. The ratio of the number of pixels associated with stellar ages younger than 16 Myr to the total number of pixels within a hole ($f_{\rm YOUNG}$) does not correlate with the hole properties.
2. The dynamical ages of the holes are generally higher than the younger burst by a factor of 5. The hole dynamical age is, however, an upper limit, as it was computed by Walter & Brinks (1999) assuming a constant expansion rate. In reality, the hole expansion is expected to have been faster during its earlier phases.
3. The kinetic energy of the holes is, on average, 10% of the total energy released by the younger burst. This energy ratio (i.e., the efficiency of stellar feedback) is in agreement with the value (10%–20%) obtained by Cole et al. (1994) from fitting the galaxy luminosity functions and colors, while Bradamante et al. (1998) determined a value of 3% for supernovae Type II and 100% for supernovae Type Ia from the modeling of the chemical evolution of blue compact galaxies.

Even at the remarkable photometric depth of the LBT data, we do not find a clear one-to-one association between the observed H I holes and the most recent bursts of star formation. However, the stars formed during the younger burst do, in principle, release enough energy to power the expansion of the H I holes. In order to better investigate this apparent discrepancy, we map IC 2574 in the optical and in H I with a set of control apertures equivalent in size to the beam of the radio observations (136 pc). No observed H I hole is included among the control apertures. For those apertures with $f_{\rm YOUNG} > 70\%$ (just to focus on the interplay between the younger stellar component and the H I gas), we measure their average H I velocity dispersion $\sigma_{\rm H\,I}$ (from the second moment map of Walter & Brinks 1999), their average H I column density $\Sigma_{\rm H\,I}$, the total stellar energy of their stellar populations younger than 16 Myr $E_{\rm YOUNG}$, and the H I kinetic energy $E_{\rm H\,I}$, defined as $E_{\rm H\,I} = 1.5 \Sigma_{\rm H\,I} ({\rm area}) \sigma^2_{\rm H\,I}$ (where area is the area of the apertures). For two-thirds of the control apertures, the ratio $E_{\rm H\,I}/E_{\rm YOUNG}$ is lower than 100% and has an average value of 35%; all the remaining apertures have $E_{\rm H\,I}/E_{\rm YOUNG} > 100\%$ and are systematically associated with $\Sigma_{\rm H\,I} \geq 8 \times 10^{20}$ cm^{-2}. Once again, the stellar populations formed during the younger burst could balance the kinetic energy stored in the H I gas, transform it into an expansion motion, and thus produce a detectable H I hole for most of the control apertures. Yet these regions failed to develop a H I hole. These same stellar populations could also sustain the H I noncircular motions, since their average ratio $E^{\rm ncir}_{\rm H\,I}/E_{\rm YOUNG}$ is 21%.

Holes in the H I distribution may also be formed by ionization due to the UV emission of the young stars. In the case of those control apertures with $f_{\rm YOUNG} > 70\%$, the Strömgren sphere produced by their stellar populations younger than 16 Myr is 4 times bigger in radius than the apertures and, therefore, would produce a detectable H I hole. Since this is not observed, the fraction of ionizing photons that effectively ionize the H I gas has to be rather small; a fraction $\leq$20% of the total number of ionizing photons emitted by the young stellar populations reduces the radius of the Strömgren sphere to $\leq$2 times the aperture radius, making any H I hole formed via ionization less likely to be detectable. This result is in agreement with the lack of correlation between star formation activity and H I density seen in § 4.3, indicating that star formation does not appear to significantly affect the properties of the H I gas in IC 2574. From the analysis of the stellar content of the H I holes and the control apertures, it is hard to establish whether stellar/supernova feedback is at work in IC 2574 on local scales of a few hundred parsecs; this same result has been found for other dwarf galaxies (LMC and SMC, Kim et al. 1999, Hatzidimitriou et al. 2005; M33, van der Hulst 1996; Holmberg II, Rhode et al. 1999). The ultimate explanation of these findings remains elusive; it may rest either in an overestimate of the stellar mass loss and stellar winds, especially at low metallicity, or in our understanding of how stellar energy interacts with the ISM. Another explanation may be found in a stochastic sampling of the IMF in low-mass stellar systems. Stellar population synthesis codes usually assume that the IMF is a densely sampled probabilistic distribution function, while it is in reality poorly and discretely sampled in low-mass stellar systems. This assumption produces fluctuations in the predicted properties of these systems which may mislead comparisons with the observations (Cerviño & Valls-Gabaud 2003), for example, by overestimating the stellar energy released to the ISM and thus underestimating the efficiency of stellar feedback. As shown by Cerviño & Molla (2002), Cerviño & Luridiana (2006), and Carigi & Hernandez (2008), stochastic effects on the IMF sampling become significant in low-metallicity systems such as dwarf galaxies.

We would like to thank S.-H. Oh for making available the map of the kinetic energy associated with noncircular motions in IC 2574 and P. Smith for assisting with the observations. Based on data acquired using the Large Binocular Telescope (LBT). This research made use of tools provided by Astrometry.net. The LBT is an international collaboration among institutions in the United States, Italy, and Germany. LBT Corporation partners are the University of Arizona, on behalf of the Arizona university system; Istituto Nazionale di Astrofisica, Italy; LBT Beteiligungsgesellschaft, Germany, representing the Max Planck Society, the Astrophysical Institute Potsdam, and Heidelberg University; The Ohio State University; and the Research Corporation, on behalf of the University of Notre Dame, University of Minnesota, and University of Virginia.

REFERENCES

Allen, R. J., Knapen, J. H., Bohlin, R., & Stecher, T. P. 1997, ApJ, 487, 171
Bigiel, F., Leroy, A., Walter, F., Brinks, E., de Blok, W. J. H., Madore, B., & Thornley, M. 2008, AJ, submitted
Blain, A. W., Smail, I., Ivison, R. J., Kneib, J.-P., & Frayer, D. T. 2002, Phys. Rep., 369, 111
Bouchet, P., Lequeux, J., Maurice, E., Prevot, L., & Prevot-Burnichon, M. L. 1985, A&A, 149, 330
Bradamante, F., Matteucci, F., & D'Ercole, A. 1998, A&A, 337, 338
Bureau, M., & Carignan, C. 2002, AJ, 123, 1316
Calzetti, D. 2001, PASP, 113, 1449
Cannon, J. M., et al. 2005, ApJ, 630, L37
Cardelli, J. A., Clayton, G. C., & Mathis, J. S. 1989, ApJ, 345, 245
Carigi, L., & Hernandez, X. 2008, MNRAS, in press (arXiv: 0802.1203)
Cerviño, M., & Luridiana, V. 2006, A&A, 451, 475
Cerviño, M., & Molla, M. 2002, A&A, 394, 525
Cerviño, M., & Valls-Gabaud, D. 2003, MNRAS, 338, 481
Cole, S., Aragón-Salamanca, A., Frenk, C. S., Navarro, J. F., & Zepf, S. E. 1994, MNRAS, 271, 781
Dale, D. A., et al. 2007, ApJ, 655, 863
de Blok, W. J. G., & Walter, F. 2006, AJ, 131, 363
Dib, S., Bell, E., & Burkert, A. 2006, ApJ, 638, 797
Drissen, L., Roy, J.-R., & Moffat, A. F. J. 1993, AJ, 106, 1460
Efremov, Y. N., Elmegreen, B. G., & Hodge, P. W. 1998, ApJ, 501, L163
Elmegreen, B. G. 2002, ApJ, 577, 206
Elmegreen, B. G., & Efremov, Y. N. 1998, in ASP Conf. Ser., The Orion Complex Revisited, ed. M. J. McCaughrean & A. Burkert (San Francisco: ASP), preprint (astro-ph/9801071)
Giallongo, E., et al. 2008, A&A, 482, 349
Hatzidimitriou, D., Stanimirovic, S., Maragoudaki, F., Staveley-Smith, L., Dapergolas, A., & Bratsolis, E. 2005, MNRAS, 360, 1171
Heckman, T. M. 1998, in ASP Conf. Ser. 148, Origins, ed. C. E. Woodward, J. M. Shull, & H. A. Thronson, Jr. (San Francisco: ASP), 127
Hill, J. M., Green, R. F., & Slagle, J. H. 2006, Proc. SPIE, 6267, 62670Y
Kennicutt, R. C. 1989, ApJ, 344, 685
———. 1998a, ARA&A, 36, 189
———. 1998b, ApJ, 498, 541
Kennicutt, R. C., et al. 2007, ApJ, 671, 333
Kim, S., Dopita, M. A., Staveley-Smith, L., & Bessell, M. S. 1999, AJ, 118, 2797
Kroupa, P. 2001, MNRAS, 322, 231
Leitherer, C., Robert, C., & Drissen, L. 1992, ApJ, 401, 596
Leitherer, C., et al. 1999, ApJS, 123, 3
Leroy, A., Walter, F., Bigiel, F., Brinks, E., de Blok, W. J. H., Madore, B., & Thornley, M. 2008, AJ, submitted
Loeb, A., & Perna, R. 1998, ApJ, 503, L35
Martimbeau, N., Carignan, C., & Roy, J.-R. 1994, AJ, 107, 543
Meynet, G., Maeder, A., Schaller, D., & Charbonnel, C. 1994, A&AS, 103, 97
Miller, B. W., & Hodge, P. 1994, ApJ, 427, 656
Oh, S.-H., de Blok, W. J. G., Walter, F., Brinks, E., & Kennicutt, R. C. 2008, ApJ, submitted
Osterbrock, D. E. 1989, Astrophysics of Gaseous Nebulae and Active Galactic Nuclei (Mill Valley: University Science Books)
Pasquali, A., & Castangia, P. 2008, MNRAS, 385, 468
Pasquali, A., de Grijs, R., & Gallagher, J. S. 2003, MNRAS, 345, 161
Pettini, M., Shapley, A. E., Steidel, C. C., Cuby, J.-G., Dickinson, M., Moorwoood, A. F. M., Adelberger, K. L., & Giavalisco, M. 2001, ApJ, 554, 981
Ragazzoni, R., et al. 2006, Proc. SPIE, 6272, 62720T
Rhode, K. L., Salzer, J. J., Westpfahl, D. J., & Radice, L. A. 1999, AJ, 118, 323
Robert, C., Leitherer, C., & Heckman, T. M. 1993, ApJ, 418, 749
Schaye, J. 2004, ApJ, 609, 667
Schlegel, D. J., Finkbeiner, D. P., & Davis, M. 1998, ApJ, 500, 525
Schmidt, M. 1959, ApJ, 129, 243
———. 1963, ApJ, 137, 758
Scott, S. E., et al. 2002, MNRAS, 331, 817
Shaya, E. J., & Federman, S. R. 1987, ApJ, 319, 76
Silk, J. 1997, ApJ, 481, 703
Skillman, E. D. 1987, in Star Formation in Galaxies, ed. C. J. L. Persson (Washington: NASA), 263
Steidel, C. C., Giavalisco, M., Pettini, M., Dickinson, M., & Adelberger, K. L. 1996, ApJ, 462, L17
Stewart, S. G., & Walter, F. 2000, AJ, 120, 1794
Tamburro, D. 2008, Ph.D. thesis, Univ. Heidelberg
Tenorio-Tagle, G. 1980, A&A, 88, 61
———. 1981, A&A, 94, 338
Tilanus, R. P. J., & Allen, R. J. 1991, A&A, 244, 8
Tomita, A., Ohta, K., Nakanishi, K., Takeuchi, T. T., & Saito, M. 1998, AJ, 116, 131
van der Hulst, T. 1996, in ASP Conf. Ser. 106, Minnesota Lectures on Extragalactic Neutral Hydrogen, ed. E. D. Skillman (San Francisco: ASP), 47
Walter, F., & Brinks, E. 1999, AJ, 118, 273
Walter, F., Kerp, J., Duric, N., Brinks, E., & Klein, U. 1998, ApJ, 502, L143
Walter, F., et al. 2007, ApJ, 661, 102
Weedman, D. 1991, in Massive Stars in Starbursts, ed. C. Leitherer et al. (Cambridge: Cambridge Univ. Press), 317
Wong, T., & Blitz, L. 2002, ApJ, 569, 157